Marine-inspired molecular mimicry generates a drug-free, but immunogenic hydrogel adhesive protecting surgical anastomosis

Jinjian Huang[a], Yungang Jiang[a], Ye Liu[a], Yanhan Ren[b], Ziyan Xu[a,c], Zongan Li[d], Yun Zhao[e], Xiuwen Wu[a], Jianan Ren[a,*]

[a] PLA Key Laboratory of Trauma and Surgical Infections, Research Institute of General Surgery, Jinling Hospital, School of Medicine, Southeast University, Nanjing, 210009, China
[b] Chicago Medical School, Rosalind Franklin University of Medicine and Science, North Chicago, IL 60064, USA
[c] School of Medicine, Nanjing University, Nanjing, 210093, China
[d] Jiangsu Key Laboratory of 3D Printing Equipment and Manufacturing, NARI School of Electrical and Automation Engineering, Nanjing Normal University, Nanjing, 210042, China
[e] Gastrointestinal Unit and Center for the Study of Inflammatory Bowel Disease, Massachusetts General Hospital, Harvard Medical School, Boston, MA, 02114, USA

ARTICLE INFO

ABSTRACT

Herein, we report the synthesis of a biomimic hydrogel adhesive that addresses the poor healing of surgical anastomosis. Dopamine-conjugated xanthan gum (Da-g-Xan) is fabricated using deep insights into the molecular similarity between mussels' adhesive and dopamine as well as the structural similarity between barnacle cement proteins and xanthan gum. The hydrogel mimics marine animals' adherence to wet tissue surfaces. Upon applying this adhesive to colonic anastomosis in a rat model, protective effects were shown by significantly improving the bursting pressure. Mechanistically, the architecture of Da-g-Xan hydrogel is maintained by dynamic intermolecular hydrogen bonds that allow the quick release of Da-g-Xan. The free Da-g-Xan can regulate the inflammatory status and induce type 2 macrophage polarization (M2) by specifically interacting with mannose receptors (CD206) revealed by RNA-sequencing and molecular binding assays. Consequently, an appropriate microenvironment for tissue healing is created by the secretion of chemokines and growth factors from M2 macrophages, strengthening the fibroblast migration and proliferation, collagen synthesis and epithelial vascularization. Overall, this study demonstrates an unprecedented strategy for generating an adhesive by synergistic mimicry inspired by two marine animals, and the results show that the Da-g-Xan adhesive augments native tissue regenerative responses, thus enabling enhanced recovery following surgical anastomosis.

1. Introduction

Postoperative anastomotic leakage (PAL) is a "nightmare scenario" for patients and surgeons after gastrointestinal surgery. The incidence of PAL is reported to be 7%–12% for gastroesophageal surgery and 3%–19% for colorectal surgery [1,2]. It is estimated that every year at least 1.3 million patients worldwide will experience complications involving with PAL after surgical procedures [3]. Symptomatic PAL is a severe clinical syndrome featuring loss of digestive fluids, malnutrition, local and systemic infections, and even death. Existing management strategies for PAL include drainage, antibiotics, and re-laparotomy with their attendant costs and morbidity [4]. For prevention of PAL, surgeons have employed a series of approaches including improved surgical technology, preoperative mechanical bowel preparation and oral antibiotics, but studies have shown that more than half of patients do not benefit from these interventions [5,6]. Until now, the poor healing of surgical anastomosis has posed an intractable problem to clinical practice.

Hydrogels remain the most popular scaffolds in the repair of injured digestive tracts because they mimic three-dimensional networks of extracellular matrix and support cell infiltration and tissue regeneration [7,8]. Two main strategies of hydrogel application are promising: acellular scaffolds and cell-laden scaffolds. Translational attempts of cell-laden scaffolds are being hampered because of (i) inconvenience of the preparation process, (ii) diversity of cell types, (iii) alteration of cell phenotypes, and (iv) difficulties of *in vivo* cell tracing [9–11]. Acellular scaffolds are easily fabricated and user-friendly, which enables them to have a rapid clinical translation. However, they also have several

---

specific drawbacks. First, hydrogels can potentially detach from the *in vivo* targeted sites with wet tissue surfaces [12]. Second, covalently-crosslinked hydrogels are slowly degraded and are prone to foreign body responses, leading to fibrosis and encapsulation [13]. Third, inorganic polymers used in hydrogel synthesis lack definite bioactivities, and have to experience complicated modifications of active molecules for tissue engineering [14,15]. Therefore, research priority should be given to developing tissue-attachable, degradable, and bioactive hydrogel adhesives.

Marine animals have inspired researchers to invent adhesives based on various mechanisms. For example, mussels can attach to wet surfaces using the byssal threads and terminal pads where mussel foot proteins (mfps) are widely distributed. The mfps contain up to 27 mol% of L-3,4-dihydroxyphenylalanine (DOPA), and the specific catechol groups in DOPA serve as the functional components that mediate underwater adhesion [16]. Another relevant marine animal is the barnacle. Its strong underwater adhesion is attributed to secreted cement proteins with specific amyloid nanostructures [17]. Such structures are characterized by interlaced fibers for increase of contact area [18]. By using microbial genetic engineering, several studies have designed a new generation of marine-inspired adhesives that combine two or more independent natural adhesion systems, but their methods of synthesis are complex, low-yield and prone to microbial exposure [19,20]. As an alternative and flexible approach, molecular mimicry can be utilized to engineer molecules that share structural and functional similarities to the originals, and this has been applied in fields ranging from chemical synthesis [21] to autoimmune activation [22]. However, the rational design of adhesives based on molecular mimicry remains challenging and has not been fully demonstrated, in part due to limited understanding of similarities between existing polymers and marine-derived molecules.

Xanthan gum is a natural exo-polysaccharide produced by the microorganism *Xanthomonas campestris*. This polysaccharide has two types of secondary structures (ordered helix structure and disordered coil structure) depending on pH, ionic strength, and temperature. The ordered conformation of xanthan gum been identified as interlaced molecular chains connected by dense hydrogen-bonding networks in which each single chain is formed with an intrinsic double-stranded helix [23,24]. This mimics the amyloid nanostructures of barnacle cement proteins and enlarges the contact area of xanthan gum chains to substrates. Apart from structure mimicry, molecular formula mimicry is more direct and feasible. Dopamine is an analogue of DOPA. The catechol groups in dopamine can act as functional groups that execute mussel-inspired underwater adhesion [25,26]. Given the two different marine animal-inspired adhesion mechanisms, an alliance of xanthan gum and dopamine could in theory be used to develop stronger underwater adhesives.

In addition, advantageous tissue adhesives should have specific bioactivities in the improvement of tissue healing. To our knowledge, postoperative tissue repair is accompanied by and also partially regulated by inflammatory responses from various leukocyte lineages [27]. Among such cells, macrophages play a crucial role since they can regulate inflammation by alteration of cellular polarization. Type 1 macrophage polarization (M1) is effective at killing microbes and producing inflammatory cytokines, but also has the potential to cause toxicity and collateral tissue damage. In contrast, type 2 macrophage polarization (M2) preserves tissue function under physiological conditions, resolves inflammation after injury, and promotes repair during wound healing [28]. Studies have revealed that xanthan gum composite materials play an important role in tissue engineering, but the underlying mechanisms are poorly understood [29]. An up-to-date work by Liu et al. [30] indicates that xanthan gum can reduce the inflammation of macrophages upon lipopolysaccharide stimulation, which inspires us to investigate the functions of xanthan gum and its derivatives on the regulation of macrophage polarization and the potential molecular basis.

To satisfy the critical requirements for wet tissue attachability and

surgical anastomosis healing, we herein developed a novel marine-inspired hydrogel adhesive based on dopamine-conjugated xanthan gum (Da-g-Xan). Da-g-Xan exhibited enhanced dynamic intermolecular hydrogen-bonding interactions that not only maintained the three-dimensional network of the hydrogel, but also imbued it with degradability, self-healing, injectability, and strong adhesive strength. Notably, we found that released Da-g-Xan from degradation bound to mannose receptors (CD206) and mediated M2 macrophage polarization through increasing the phosphorylation of extracellular regulated protein kinase (ERK) signaling. In this way, this hydrogel promoted the paracrine action of macrophages by raising the secretion of growth factors and chemokines, consequently promoting the proliferation, migration, and collagen synthesis of fibroblasts as well as epithelial vascularization to repair gastrointestinal injury.

2. Materials and methods

2.1. Sources of materials, cell lines and animals

Xanthan gum (viscosity of 1%wt aqueous solution at 20 °C: 1450-2000 mPa s) was purchased from TCI Development Co., Ltd, Japan. Dopamine hydrochloride was purchased from Sigma-Aldrich, USA. 1-Ethyl-3-(3-dimethylaminopropyl)- carbodiimide (EDC), N-hydroxysuccinimide (NHS), and 5-Isothiocyanato fluorescein (5-FITC) were purchased from Aladdin Co., Ltd, China. 1,8-Diazabicyclo[5.4.0]undec-7-ene (DBU) was purchased from Sinopharm Chemical Reagent Co., Ltd, China. All other reagents were of analytical reagent grade.

Raw264.7 cell line and L929 cell line were purchased from KeyGEN BioTech Co., Ltd in China, and cultured in DMEM containing 10% FBS and 1% penicillin/streptomycin at 37 °C in a moist atmosphere (5% CO2, 95% air). Bone marrow-derived macrophages (BMDMs) were isolated from C57BL/6 mice and differentiated according to the previous protocol [31].

Eight-week-old male C57BL/6 mice and seven-week-old male Sprague Dawley rats were provided by Jinling Hospital and were raised at 25 °C under natural light–dark cycles with free access to food and water. Chloral hydrate was used to carry out anesthesia through intraperitoneal injection at the dose of 40 mg/100g of body weight. Rats were fasting from 12 h before surgery to 24 h after surgery. All the animal care and experimental protocols were performed in strict accordance with the chinese guideline for the care and use of laboratory animals (Ministry of Science and Technology [2006] file no. 398) and approved by Animal Investigation Ethics Committee of Jinling Hospital.

2.2. Synthesis of Da-g-Xan conjugate

One hundred and 20 mL of 0.6%wt xanthan gum aqueous solution were prepared by dissolving xanthan gum powders in deionized water, followed by stirring overnight in a round-bottom flask. Then, carboxyl groups of xanthan gum were activated by adding 0.272g EDC and 0.166g NHS in which the molar ratio of carboxyl groups in xanthan gum, EDC and NHS was 1:1:1. After stirring for 1 h, dopamine hydrochloride with varying molar ratios to carboxyl groups in xanthan gum at 0.5:1, 1:1, 3:1, or 6:1 was added in the amounts of 0.068 g, 0.136 g, 0.410 g, or 0.820 g, respectively. The flask was then immediately vacuumized and refilled with nitrogen. The entire solution was stirred for 24 h under nitrogen and then dialyzed for 3 d using dialysis membranes (molecular weight cut-off: 12-14 kDa) to remove unreacted residues. Finally, the solution was lyophilized in a freeze dryer (Xiongdi Instrument Co., Ltd, China) and stored in a sealed bag at 4 °C.

2.3. Characterization of Da-g-Xan conjugate and Da-g-Xan hydrogel adhesive

i) Selection of a highly-viscous biopolymer. Viscosity comparison of 2%wt biopolymer aqueous solution (e.g., alginate, carboxymethyl

chitosan, gelatin, carboxymethyl cellulose, konjac glucamannan, and xanthan gum) was carried out by using a rheometer (Anton Paar Co., Ltd, Austria) at the shear rate of 0.1 s^{-1}. ii) Confirmation of Da-to-Xan conjugation. The FTIR spectra of xanthan gum, dopamine and Da-g-Xan were recorded using a Nicolet-6700 spectrometer (Thermo, USA). The NMR spectra of xanthan gum, dopamine, and Da-g-Xan dissolved in deuterated solvents were characterized by ^{1}H NMR (Bruker, Germany). The conjugation efficiency of the Da-to-Xan side chain was determined using an UV–vis spectrophotometer (PerkinElmer, USA) by measuring the absorbance at 280 nm of Da-g-Xan solution with known concentrations and then calculated from a calibration curve of dopamine: y = 2630x + 0.0069 (r^2 = 0.999). iii) Morphology. Porosity of 10%wt Xan gum and 10 wt% Da-g-Xan was observed using a scanning electron microscope (SEM, Hitachi, Japan). Conformation of Da-g-Xan was illustrated by circular dichroism (CD) spectra of 10 mg/mL of xanthan gum solution, 0.15 mg/mL dopamine solution and 10 mg/mL of Da-g-Xan solution using a CD spectrometer (Jasco Co., Ltd, Japan). Moreover, atomic force microscopy (AFM, Bruker, Germany) was used to visualize the molecular morphology of 10 μL of 1 μg/mL xanthan gum or Da-g-Xan aqueous solution treated with air drying overnight on mica plates. iv) Adhesive force test. The adhesive strength of Da-g-Xan hydrogels for fresh porcine skin was investigated by the lap-shear strength test with a universal testing machine (MTS CMT2103, USA) as described previously [32]. v) Self-healing property. This characteristic was demonstrated by the rapid healing of hydrogels after cutting and was confirmed by a recovery test using a rheometer in which the alternate step strain switched from a small strain (1%) to a large strain (300%) in continuous step strain measurements at a fixed angular frequency (10 rad/s). vi) Injectability. An extrusion-based 3D printer (Baoyan Co., Ltd, China) was used to show the injectability of Da-g-Xan using blue chromogenic agents. Moreover, the shear-thinning property of 10%wt xanthan gum or Da-g-Xan aqueous solution was investigated using a rheometer at shear rates from 0.1 to 500 s^{-1}. vii) Storage modulus (G') and loss modulus (G"). These two parameters of 10%wt xanthan gum and 10%wt Da-g-Xan were measured with a rheometer in the dynamic oscillatory mode with the constant strain at 1% and frequency at 10 Hz viii) Degradation. The degradation of 10%wt xanthan gum or 10%wt Da-g-Xan hydrogel was determined by a soaking method using PBS at 37 °C and was calculated from the ratio of remaining mass to original mass.

2.4. RNA-seq

Raw264.7 macrophages (1 × 10^6 cells/mL) were treated with Da-g-Xan at 20 μg/mL for 24 h before the total mRNA samples were extracted by Trizol (Sigma-Aldrich, USA), and raw264.7 macrophages without any treatment were used as a control. Each intervention was in triplicate. The libraries were constructed by using an NEBNext Ultra RNA Library Prep Kit (CapitalBio Technology, Beijing, China) and were sequenced on a HiSeq XTen system (Illumina, San Diego, USA). The reads were mapped to the reference using Hisat, and differential expression analysis was performed using the R package DESeq2 in which genes with log$_2$(fold change) > 1 were regarded as statistically significantly different. Moreover, enrichment analysis was conducted for all genes in the GO database, the KEGG database and the Reactome database. Raw data files and processed data files of all RNA-seq analysis have been deposited in the SRA database (accession PRJNA625852).

2.5. Flow cytometry

Raw264.7 macrophages and BMDMs (1 × 10^6 cells/mL) were treated with interferon-γ (IFN-γ) at 20 ng/mL for 2 h. Da-g-Xan at 1, 5, or 20 μg/mL was added, and cells without Da-g-Xan were considered as controls. Twenty-four hours later, cells were collected and incubated with CD11b (0.25 μg/test, Invitrogen, 56-0112-82), CD86 (0.125 μg/test, Invitrogen, 12-0862-82) and CD206 (1 μg/mL, abcam, ab195191).

Then, cells were measured using a BD FACSCalibur CellSorting System (BD Bioscience, USA) and analyzed with FlowJo software (Tree Star Inc, USA). This experiment was performed in triplicate. Dissected tissues from rat colonic anastomosis were washed with Hanks Balanced Salt Solution (HBSS) for three times and minced into 1-2 mm pieces. The tissue pieces were digested with 2 mL GEXSCOPETM Tissue Dissociation Solution (Singleron, China), and the red blood cells were removed with 2 mL GEXSCOPETM red blood cell lysis buffer (Singleron, China). The resulting cells were stained with CD 206 (1 μg/mL, abcam, ab125028) with secondary donkey anti-rabbit antibodies (1 μg/mL, abcam, ab150075), CD11b (2 μg/mL, BD Biosciences, cat. 554862), CD86 (2.5 μg/mL, BD Biosciences, cat. 561961) and then measured using the CellSorting System.

2.6. ELISA

TNF-α, IL-1β, IL-10, IL-4, G-CSF and TGF-β1 levels in culture supernatants were measured using a Mouse TNF-α ELISA Kit (MULTI SCIENCES, China), Mouse IL-1β ELISA Kit (MULTI SCIENCES, China), Mouse IL-10 ELISA Kit (Angle Gene, China), Mouse IL-4 ELISA Kit (Angle Gene, China), Mouse G-CSF/CSF3 ELISA Kit (Sigma-Aldrich, USA), and mouse TGF-β1 ELISA kit (KeyGEN BioTech Co., Ltd, China). Moreover, IFN-γ levels in intestinal tissues were measured using a rat IFN-γ ELISA kit (MULTI SCIENCES, China).

2.7. q-PCR

Raw264.7 macrophages and BMDMs were resuspended in Trizol to extract RNA. Then, mRNA was quantified by qPCR using the primers listed in Table S1. The mRNA expressions were normalized to GAPDH.

2.8. Computer simulation of binding affinity

Three types of monomers of Da-g-Xan were drawn in ChemDraw Professional 16.0 and saved as SMILES. The files were converted into PDB form using a free website: https://www.mn-am.com/online_demos/corina_demo. The PDB file of CD206 was downloaded from the following website: https://www.uniprot.org/uniprot/P22897. Autodock Vina was used to simulate binding sites between the monomers of Da-g-Xan and the single lectin-responsive site of CD206 and calculate the corresponding binding energy.

2.9. Immune dot-blots

To synthesize 5-FITC-conjugated Da-g-Xan (Da-g-Xan-FITC), 1 μg/mL of Da-g-Xan carbonate buffer solution was reacted with 5-FITC, shielded from light, and stirred for 12 h, in which the mass ratio of Da-g-Xan to FITC was 1:10. DBU was added as a catalyst. After the reaction, the whole solution was dialyzed and lyophilized. One microliter of 1 μg/μL CD206 recombinant proteins (R&D systems, Q2HZ94) was spotted on pre-equilibrated polyvinylidene fluoride (PVDF) membranes, and PBS without CD206 was used as a control. The membranes were dried, blocked with BSA (5% in PBS) for 1 h and rinsed with PBS three times, followed by incubation with Da-g-Xan-FITC at different concentrations of 1, 5, 20 and 100 μg/mL for 4 h at 37 °C. Then, the blots were washed three times, dried and scanned using a Bio-Spectrum Imaging System (BD Biosciences, USA).

2.10. Immunofluorescence

To observe the cell morphology, raw264.7 macrophages were cultured with 20 μg/mL Da-g-Xan for 4 h and then washed with PBS three times. Then, cells were fixed with 4% (w/v) paraformaldehyde for 30 min at room temperature, followed by 0.05% (w/v) Triton X-100 for permeabilization. Cytoplasm was stained with β-actin (abcam, ab115777) followed by donkey anti-rabbit antibodies (abcam,
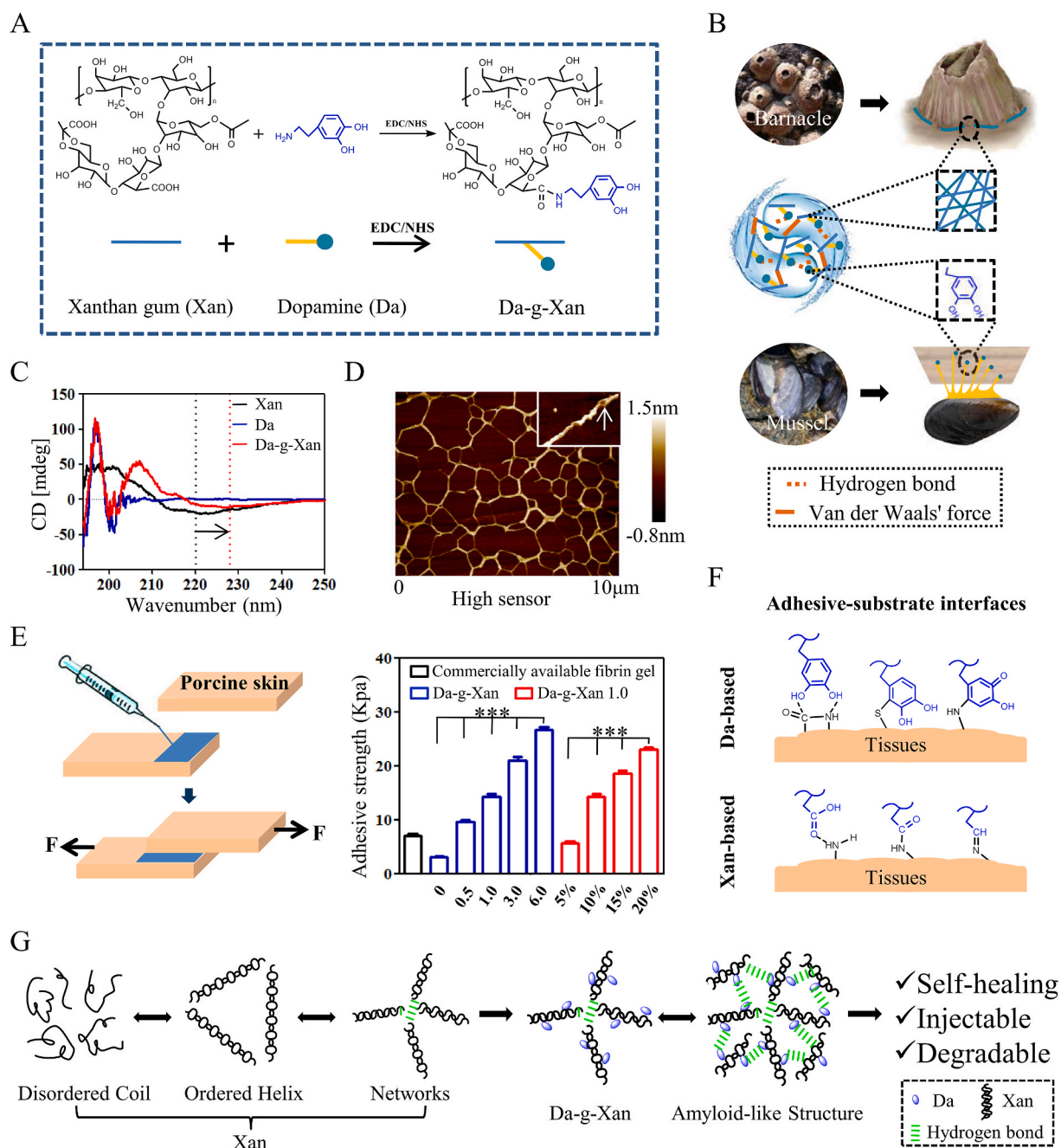
Fig. 1. Design, synthesis, characterization, and molecular basis of the Da-g-Xan hydrogel adhesive. (A) Generation of Da-g-Xan through conjugating dopamine (Da) to xanthan gum (Xan) via the activation of carboxyl groups by EDC/NHS catalysts. (B) Da-g-Xan simultaneously mimics the mfps of mussels and the amyloid-like structure of barnacle cement proteins to work as an adhesive. (C) The CD spectrum reveals that Da-g-Xan has a highly ordered and homogeneous conformation that is superior to xanthan gum. (D) The AFM image directly demonstrates that the Da-g-Xan chains are interlaced, and arranged like the amyloid nanostructure of barnacle cement proteins to increase the contact surface. White arrow: double-stranded helices of Da-g-Xan. (E) The adhesive strength of Da-g-Xan can be regulated by substitution degree of dopamine and the concentration of Da-g-Xan. The numbers below the blue columns represent molar ratios of dopamine hydrochloride to the carboxyl groups in xanthan gum; and the numbers below the red columns represent different concentrations of the Da-g-Xan 1.0 conjugates in the hydrogel adhesives. The Da-g-Xan 1.0 conjugates were produced from the 1:1 M ratio of dopamine hydrochloride to the carboxyl groups in xanthan gum. (F) Multiple interfacial linkages between the Da-g-Xan adhesive and tissue surface synergistically mediate the strong tissue adhesion. (G) As a summary, the enhanced intermolecular hydrogen bonds endow the Da-g-Xan hydrogel with a remodeled microstructure and desirable properties such as self-healing, injectability, and degradability.

ab150075), and nuclei were stained with DAPI (abcam, ab104139). To co-localize CD206 with Da-g-Xan, raw264.7 macrophages were cultured with 20 μg/mL of Da-g-Xan-FITC for 4 h followed by staining with CD206 (abcam, ab195192). The nuclei were also stained with DAPI (abcam, ab104139). A confocal scanning microscope (FV1000, Olympus, Japan) was used for image analysis. The colonic anastomosis samples were fixed with 4% (w/v) paraformaldehyde, embedded in

Paraffin, and then mounted on slides. The slides were treated with CD 31 (Servicebio, GB13063) and α-SMA (Servicebio, GB13044) followed by staining with donkey anti-goat antibodies (abcam, ab150135) and goat anti-mouse antibodies (Servicebio, GB22301). The images were recorded by an inverted fluorescence microscope (AXIO, ZEISS, Germany).

2.11. Electroporation and shRNA interference

CD206 shRNA and negative control shRNA were designed by using GenePharma Designer 3.0 software; the targeting sequences are listed in Table S2. One milliliter of 2×10^6 cells/mL raw264.7 macrophages was blended with 1 μg shRNA and then electroporated using a Micro-Pulser electroporator (Bio-Rad, USA) in cuvettes.

2.12. Western blotting

Proteins from the lysed cells were separated by SDS-PAGE and transferred to PVDF membranes. The membranes were then incubated overnight at 4 °C with antibodies against CD206 (abcam, ab64693), *p*-ERK (abcam, ab201015), ERK (abcam, ab184699), collagen 1 (abcam, ab6308), collagen 3 (abcam, ab7778) and GAPDH (abcam, ab8245). Positive signals were scanned using the G:BOX chemiXR5 gel imaging system (New England BioGroup, USA). Protein bands were quantified in optical density units using the Gel-Pro32 software (Media Cybernetics, USA) and were normalized to the corresponding GAPDH bands.

2.13. Cell proliferation and migration assay

Proliferation rates of cells were determined using a cell counting kit (CCK-8, KeyGEN BioTech Co., Ltd, China). Cell migration was detected using a transwell chamber (Corning, USA) in which cells moving to the lower surface of the filter were stained by 0.1%wt cystal violet.

2.14. Colonic anastomotic model

The abdomens of rats were disinfected with iodophor three times while the rats were anesthetized, and incisions were made in the middle abdomen. The arch of mesenteric vessels along the specific transparent region and 1-2 cm distal to the ileocecal junction was dissected and ligatured. This step was important for reducing bleeding and for improving survival rates. Afterwards, colectomy and anastomosis were carried out by using 6-0 Nylon sutures (Suzhou Medical Co., Ltd, China). Rats in different groups were further treated with the commercial fibrin gel (Hangzhou Puji CO. LTD, China), the 10%wt Da-g-Xan hydrogel adhesive or with nothing as a control. The whole-animal procedures were performed by two senior surgeons and their assistants. At postoperative day (POD) 1, the anastomotic tissues of three rats in the control group along with their normal colonic tissues without any surgical procedures were harvested for detection of IFN-γ levels. At POD 7, rats in the three groups with 10 animals in each group were used to observe histological morphology, analyze macrophage polarization proportions and measure anastomotic bursting pressure using an electrocardio monitoring instrument (Instrumentarium Co., Ltd, Finland). X-ray imaging (Aolong Co., Ltd, China) was performed on rats treated with the Da-g-Xan hydrogel adhesive after transanal injection of 10 mL barium sulfate solution.

2.15. Statistical analysis

Data are shown as means ± SEM. Data were analyzed using GraphPad Prism 5 software by Student's *t*-test (unpaired and two-tailedd) or one-way ANOVA (analysis of variance), followed by Dunnett's or Bonferroni's post hoc test if needed. The values were considered significantly different when $p < 0.05$.

3. Results

3.1. Inspired by mussels and barnacles, Da-g-Xan hydrogel adhesive is synthesized and shows multiple application advantages

By comparison, we found that the viscosity of xanthan gum was the highest among the common biopolymers; the value reached 3×10^4 mPa s when the concentration of xanthan gum was 2%wt, and the external shear rate was 0.1 s^{-1} (Fig. S1). This step demonstrated that xanthan gum is an appropriate polymer for generation of adhesives. To realize the hybrid of two adhesion mechanisms, dopamine was conjugated to the carboxyl groups of xanthan gum's branched chains with a molar ratio of 1:1 to produce the Da-g-Xan conjugate (Fig. 1A), in which xanthan gum acted as a "structure-based adhesion component" of barnacles and dopamine was for a "molecule-based adhesion component" of mussels (Fig. 1B). EDC and NHS were used as catalysts to activate the carboxyl groups in xanthan gum. Owing to the presence of two carboxyl groups in each branch chain, the final reacted monomers had three forms (Fig. S2A). To confirm the conjugate, FTIR, ^{1}H NMR, and UV–vis were used to characterize the chemical structure. Fig. S2B shows the absorption peak at 1515 cm^{-1} in Da-g-Xan spectrum from the C=C in-plane vibration of a benzene ring. Fig. S2C indicates the absorption peak at 6.62–6.91 ppm referring to catechol groups of dopamine in the conjugate. UV–vis detected the catechol groups by the presence of the absorption peak at 280 nm (Fig. S2D). These results suggested that dopamine had been successfully conjugated to xanthan gum as desired.

However, it was uncertain whether any conformational alterations had occurred when the xanthan gum was conjugated by dopamine. To our knowledge, the CD spectrum of xanthan gum was reported to have a trough at around 220 nm and a peak at around 205 nm. Their amplitude and location reflected the order-disorder conformational transition [33]. As shown in Fig. 1C, the trough of Da-g-Xan was weaker and shifted to larger wavelengths compared with xanthan gum, indicating that Da-g-Xan had a more ordered structure. Consistently, the microstructure observed using AFM in Fig. 1D shows that Da-g-Xan chains were interlaced and that each single chain was in double-stranded helix form (white arrow), while Fig. S2E shows that parts of xanthan gum chains were in disordered coils rather than in ordered helices. These results implied that Da-g-Xan performed better than simple xanthan gum regarding the structural mimicry of barnacle cement proteins.

More interestingly, because of abundant intermolecular hydrogen-bond interactions, Da-g-Xan chains were crosslinked for gelation without extra crosslinkers. As shown in a tilting experiment (Fig. S3A), 5%wt Da-g-Xan solution was fixed on the bottom of an upside-down vial, and the shape was maintained unchanged after shaking by hand and subsequent more forceful centrifugation, while the shape of 5%wt xanthan gum was destroyed by the same treatment. However, when raising the concentration of Da-g-Xan and xanthan gum to 10%wt, both tolerated the shaking and centrifugation. These phenomena were in accordance with the rheological results that the storage moduli (G') were increased by the conjugation of dopamine and the increase of polymer density (Fig. S3B), because the two factors were able to enhance the intermolecular forces. The former was possibly due to the catechol groups that generated additional hydrogen bonds [25], leading to the smaller pores and denser porosity observed by SEM (Fig. S3C), and the latter was due to the reduction of molecular spacing that facilitated the formation of hydrogen bonds.

The above results confirmed that Da-g-Xan combines two adhesive mechanisms from mussels and barnacles, and that it undergoes sol-gel conversion via increasing hydrogen-bond forces. Next, we investigated the adhesive strength of the Da-g-Xan hydrogel. Given the importance of dopamine for the adhesion system, we altered the degree of substitution (DS) ranging from 4% to 16% through changing the molar ratios of dopamine to carboxyl groups in xanthan gum (Fig. S3D). Then, Da-g-Xan hydrogel adhesives were prepared by using the conjugates with different DS values or in different concentrations. As demonstrated by lap-shear strength tests (Fig. 1E), with the increase of DS and concentrations, the adhesive force of Da-g-Xan hydrogels was increased from 10 to 27 kPa, surpassing the adhesive force of commercial fibrin gels. In practice, visceral organs (e.g., liver, heart, kidney, spleen, lung and intestine) could be bonded by using the 10%wt Da-g-Xan hydrogel adhesive (Fig. S3E) due to the synergistic binding affinities of dopamine

and xanthan gum to the nucleophiles (e.g., amide, thiol and amine) of biological molecules on wet tissue surfaces. This consequently leads to the formation of multiple interfacial linkages, including hydrogen bonds, carbon-sulfur bonds, Michael addition, amide bonds, and imine bonds (Fig. 1F), which constructed the molecular basis of tissue adhesion for the Da-g-Xan hydrogel adhesive.

Moreover, the 10%wt Da-g-Xan hydrogel adhesive was injectable when applied in an extrusion-based 3D printer (Video S1) because of its shear-thinning property (Fig. S4A). After injection, this hydrogel adhesive was likely to adapt to irregular shapes of tissues *in vivo* due to the rapid self-healing performance. As depicted in Fig. S4B, two pieces of hydrogels were split and then integrated into new ones within 100 s. Rheological recovery test further demonstrated that G' of the 10%wt Da-g-Xan hydrogel adhesive could rebound rapidly to the original level once the 1% strain was resumed from 300% strain (Fig. S4C). This was possible because the hydrogen-bond interactions that maintained the architecture of the hydrogel were dynamic, unstable and reversible. This explanation also applied to our discovery that the erosion of Da-g-Xan was almost finished within 96 h *in vitro* (Fig. S4D), which was much shorter than the majority of covalently-crosslinked hydrogels. Collectively, the Da-g-Xan hydrogel adhesive is characterized by a highly-ordered amyloid-like structure, and the internal hydrogen bonds make it injectable, self-healing and degradable (Fig. 1G).

3.2. Released Da-g-Xan regulates the inflammatory status of macrophages and reverses cell phenotypes from M1 to M2 in vitro

As the non-covalent Da-g-Xan hydrogel adhesive was dissolved easily, the released conjugates might have more immediate biological effects on macrophages (Fig. S4E). To investigate it, RNA-seq was used to describe the transcriptome atlas of raw264.7 macrophages treated with 20 μg/mL Da-g-Xan for 24 h. As shown in Fig. S5A, clustering analysis of the RNA-seq data revealed that the samples showed a consistent hierarchical clustering for the biological replicates and an evident separation by Da-g-Xan treatment based on gene expression. Through the Panther enrichment analysis (Fig. 2A), we identified differentially expressed genes enriched in the immunoregulatory pathways (i-iv). Among these genes, anti-inflammatory genes were upregulated, but the pro-inflammatory genes did not have a consistent trend (Fig. 2B). This was possibly because part of the pro-inflammatory signaling was compensatorily activated in response to the anti-inflammatory signaling for maintenance of cell homeostasis. To examine this hypothesis, the changes in anti-inflammatory cytokines (e.g., IL-4, IL-10) were compared with the changes in pro-inflammatory cytokines (e.g., IL-1β, TNF-α) when macrophages were cultured with Da-g-Xan. As shown in Fig. S5B, secretion of IL-4 and IL-10 from macrophages treated with Da-g-Xan was around four times those not treated with Da-g-Xan, while there were mild increases in IL-1β and TNF-α in the treatment with Da-g-Xan. Hence, it was suggested that Da-g-Xan had immunoregulatory effects on macrophages, especially the inhibition of inflammation.

Moreover, it was observed through fluorescence microscopy that the shapes of raw264.7 macrophages became asymmetric by the stimulation with Da-g-Xan (Fig. S5C), implying that Da-g-Xan could induce the polarization of macrophages. To investigate which type of cell polarization occurred (M1 or M2), we established IFN-γ pretreated macrophage models, because in surgical anastomosis, IFN-γ is naturally secreted in large quantities (Fig. 2C and Fig. S5D), and is a strong stimulant for M1 polarization [34]. When these raw264.7 macrophages were further treated with Da-g-Xan, M1 polarization was strikingly reversed into M2 polarization as CD206 expression was increased and CD86 expression was reduced as indicated by flow cytometry (Fig. 2D and E). It was further confirmed by qPCR analysis that the mRNA levels of M1 biomarkers (e.g., iNOS, IL-1β, IL-6, and TNF-α) were significantly decreased and the mRNA levels of M2 biomarkers (e.g., IL-10, CCL22, TGF-β and PDGF) were significantly increased because of the Da-g-Xan

treatment (Fig. 2F). Apart from the tumor-derived cell line (raw264.7), Da-g-Xan exhibited similar competence on primary macrophages (BMDM) in triggering M2 polarization from M1 polarization (Fig. S6). Therefore, the results strongly suggest that Da-g-Xan regulated the inflammatory status of macrophages and induced M2 polarization in the presence of injury-associated IFN-γ.

3.3. CD206 is the specific binding receptor of Da-g-Xan and mediates M2 macrophage polarization through ERK signaling

Little was known regarding the molecular basis of the biological effects of Da-g-Xan on macrophages. To explore it, we screened the carbohydrate binding molecules in the GO analysis, because Da-g-Xan essentially belongs to carbohydrate derivatives, and those were in the top 30 significantly different molecule functions when macrophages were treated with Da-g-Xan (Fig. S7). It was found that clec4n (dectin-2), mrc1 (CD206), and clec2d were the top three significantly upregulated genes in carbohydrate binding molecule enrichment (Fig. 3A), and they could encode c-type lectin receptors for recognition of specific carbohydrate components. In detail, dectin-2 was the binding receptor of α-mannans [35], CD206 recognized N-acetyl galactosamine and mannose of glycoproteins [36], and clec2d bound sulfated glycosaminoglycans [37], indicating that CD 206 was likely to bind Da-g-Xan because it has two non-adjacent mannoses in each branched chain. To confirm this, Autodock Vina was used for simulation of interactions between three types of Da-g-Xan monomers (Fig. S2A) and CD206. The results indicated moderate affinity between the two, with the binding energy of 7.2–7.4 kcal/mol (Fig. 3B). Moreover, CD206 expression of macrophages was significantly elevated by increasing Da-g-Xan concentrations and prolonging the culture time (Fig. 3C and Fig. S8A). Interestingly, this phenomenon was not due to xanthan gum alone, but rather to the synergism of xanthan gum and dopamine. To trace Da-g-Xan during cell culture, FITC was linked by the reaction shown in Fig. S8B. The emerging peak at 492 nm in the UV–vis spectrum suggested the success of FITC conjugation (Fig. S8C). Immunofluorescent staining revealed the co-localization of CD206 and Da-g-Xan in the cell membrane and cytoplasm of raw264.7 macrophages (Fig. 3D), implying that as an endocytic receptor with high performance in antigen presentation, CD206 could transport Da-g-Xan from the extracellular to the intracellular space. This process was realized by directly binding Da-g-Xan to CD206, as the immune dot-blot assay showed that CD206 could capture Da-g-Xan *in vitro* (Fig. 3E).

To illustrate the biological functions of CD206, this receptor was knocked down by electroporation-assisted shRNA interference. Through quantification of CD206 mRNA, it was found that shRNA 1 had the highest inhibiting efficiency (Fig. S8D). The macrophages with CD206 knocked down by shRNA 1 were then cultured with IFN-γ for 2 h, followed by treatment with Da-g-Xan for 24 h. Interestingly, the mRNA levels of M1 biomarkers (e.g., iNOS, IL-1β, IL-6, and TNF-α) were significantly elevated and the mRNA levels of M2 biomarkers (e.g., IL-10, CCL22, TGF-β, and PDGF) were significantly reduced for CD206 knockdown macrophages in comparison to normal macrophages (Fig. 3F). This result demonstrated the decisive role of CD206 in Da-g-Xan-induced M2 polarization of macrophages. Moreover, several studies have reported that extracellular regulated protein kinase (ERK) signaling was the downstream pathway regulated by CD 206 to induce M2 polarization [38,39]; therefore we verified whether this signaling was responsible for the biological behavior of Da-g-Xan. As shown in Fig. 3G and Fig. S8E, with the increase of Da-g-Xan, the phosphorylation of ERK (*p*-ERK) was increased. However, once the CD206 receptor was inhibited, the amount of *p*-ERK was decreased, indicating that Da-g-Xan could lead to *p*-ERK mediated by CD206. Collectively, the above results confirmed that CD206 was an important receptor for recognition and signal transduction of Da-g-Xan in M2 polarization.
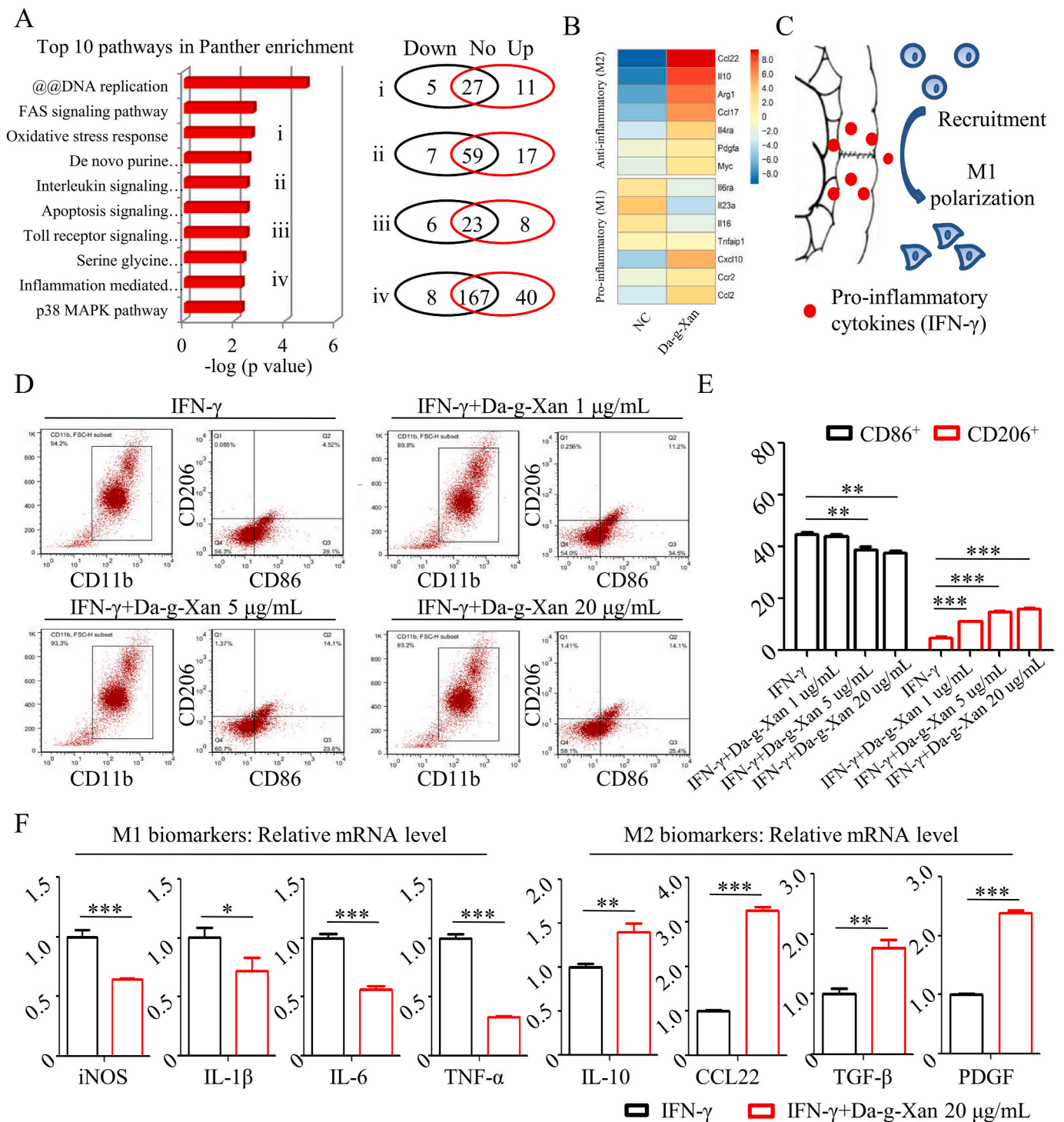
Fig. 2. Immunoregulation of released Da-g-Xan. (A) The significantly altered pathways in Panther enrichment reveal that Da-g-Xan can regulate the inflammatory responses of macrophages (left: i-iv), and the changes in gene expression of the corresponding pathways are shown on the right. (B) The alteration of typical inflammation-associated biomarkers in the heat map demonstrates the potential immunoregulatory effect of Da-g-Xan towards inflammatory suppression. (C) The schematic diagram indicates the large amount of IFN-γ inevitably secreted from the colonic anastomosis. (D) The flow cytometry results show the induction of M2 polarization of IFN-γ pretreated raw264.7 macrophages by Da-g-Xan. (E) The proportion of macrophage polarization from the flow cytometry, %; n = 3 for each replicate, **p < 0.01, ***p < 0.001. (F) The alteration of representative markers further confirms that Da-g-Xan can induce M2 polarization of IFN-γ pretreated raw264.7 macrophages; n = 3 for each replicate, *p < 0.05, **p < 0.01, ***p < 0.001.

3.4. M2 polarization triggered by Da-g-Xan improves the paracrine action of macrophages, leading to intensifying diverse functions of fibroblasts

As shown in Fig. 4A, genes were differentially expressed in the enrichment of the cell cycle and chemokines. This was possibly due to

the activation of ERK signaling by Da-g-Xan to promote cell migration and proliferation [40]. To test this hypothesis, the transwell assay and CCK-8 assay were carried out. The results indicated that with increasing Da-g-Xan concentration and culture time, the number of macrophages penetrating the membrane was increased (Fig.4B and Fig. S9A), and the
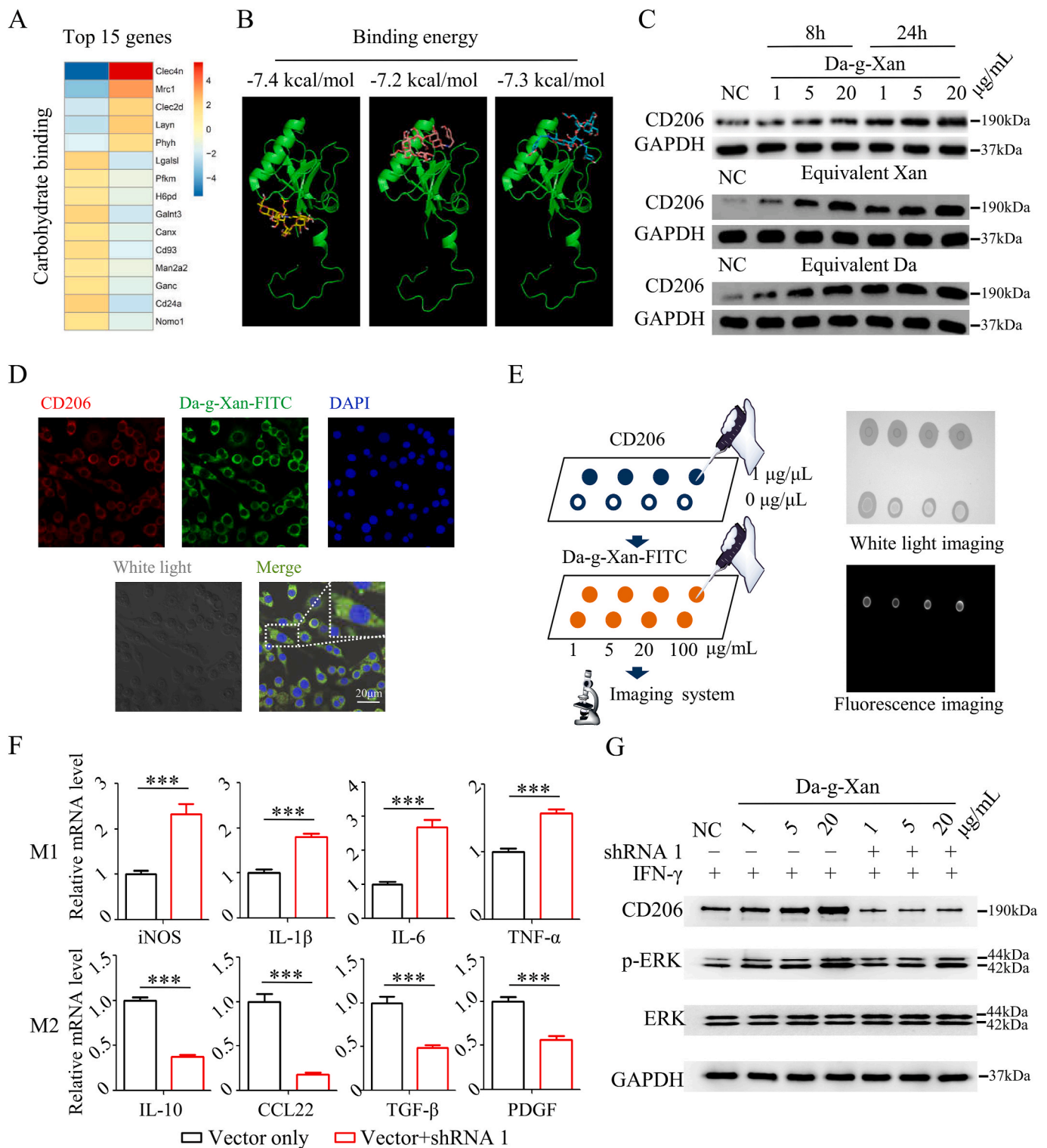
Fig. 3. CD206 mediates the recognition of Da-g-Xan and M2 macrophage polarization. (A) The fifteen most significantly changed genes of carbohydrate binding molecules in the GO analysis. (B) The computer simulation by Autodock Vina reveals the moderate affinity between different Da-g-Xan monomers and CD206. (C) The western blotting assay suggests that Da-g-Xan and its reactants, regardless of dopamine and xanthan gum, can improve the protein expression of CD206. (D) The immunofluorescent staining shows the co-localization of Da-g-Xan and CD206 in the cell membrane and cytoplasm of raw264.7 macrophages. (E) The immune dot-blotting assay suggests the specific binding of Da-g-Xan by CD 206. (F) Knockdown of CD206 by shRNA hinders the M2 macrophage polarization induced by Da-g-Xan; n = 3 for each replicate, ***p < 0.001. (G) Activation of ERK signaling is related to the M2 macrophage polarization induced by Da-g-Xan. Knockdown of CD206 slightly reduces the activation of ERK signaling and affects the macrophage polarization.

proliferative ability of macrophages was enhanced (Fig. 4C). Moreover, the chemokine G-CSF and the growth factor TGF-β were secreted in higher quantities (Fig. 4D and E), implying that the paracrine action of

macrophages was enhanced by Da-g-Xan.

Fibroblasts are the cells directly responsible tissue healing via their migration, proliferation and collagen synthesis [41]. Although it was

demonstrated for Da-g-Xan in the remodeling of macrophages, how this process influenced biological functions of fibroblasts was unknown. By using the Da-g-Xan-stimulated macrophage supernatant to culture fibroblasts, the paracrine functions of macrophages on fibroblasts could be explored. As shown in Fig. 4F and Fig. S9B, the Da-g-Xan-stimulated macrophage supernatant could maximize the migration performance of fibroblasts, although Da-g-Xan alone could also produce the effect. Likewise, the proliferative behavior of fibroblasts was strengthened by
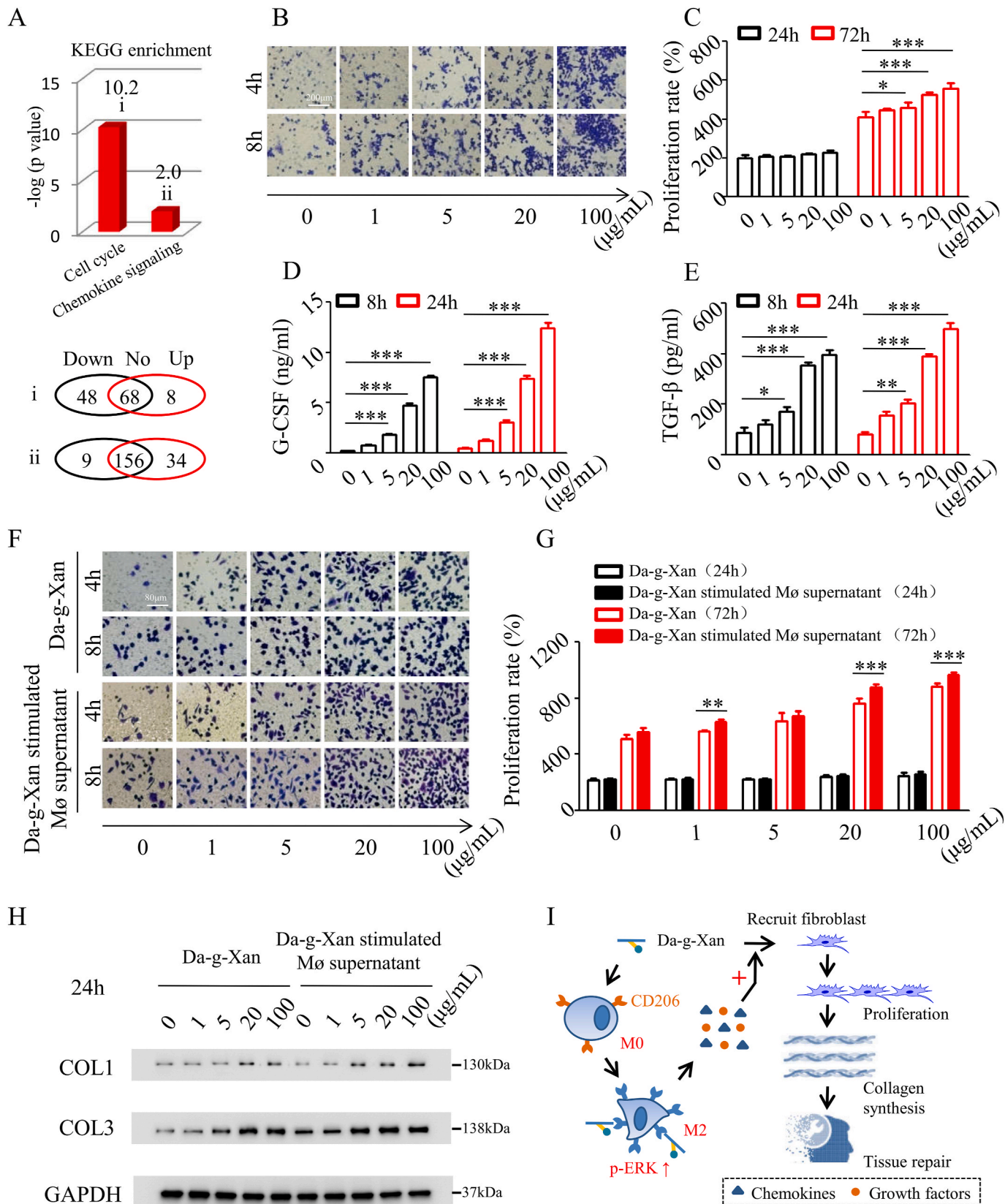
(caption on next page)

Fig. 4. Da-g-Xan creates an appropriate microenvironment for tissue repair. (A) The cell cycle pathway and chemokine signaling pathway are significantly changed by the treatment with Da-g-Xan (upper: i and ii), and the alterations in gene expression of the corresponding pathways are shown at the bottom. (B) The transwell assay reveals that the migration ability of raw264.7 macrophages is improved with increasing Da-g-Xan concentration and culture time extension. (C) The CCK-8 assay shows that the proliferative ability of raw264.7 macrophages is also improved with increasing Da-g-Xan concentration and culture time extension; n = 3 for each replicate, *p < 0.05, ***p < 0.001. (D, E) The cytokines measured by ELISA indicate that the secretion of G-CSF and TGF-β from raw264.7 macrophages is increased by increasing Da-g-Xan concentration and culture time extension; n = 3 for each replicate, *p < 0.05, **p < 0.01, ***p < 0.001. (F) The transwell assay demonstrates the paracrine action of macrophages treated with Da-g-Xan can further promote the migration of L929 fibroblasts, although Da-g-Xan alone can also induce the migration. (G) The CCK-8 assay indicates paracrine action of macrophages treated by Da-g-Xan can further improve the proliferation of L929 fibroblasts, although Da-g-Xan alone can also trigger the cell proliferation; n = 3 for each replicate, **p < 0.01, ***p < 0.001. (H) The western blotting assay suggests that paracrine action of macrophages treated with Da-g-Xan can further improve the collagen synthesis of L929 fibroblasts, although Da-g-Xan alone can also achieve collagen synthesis. (I) As a summary, Da-g-Xan has a cascade of amplification effects for fibroblasts on tissue repair mediated by the paracrine action of macrophages.

the Da-g-Xan-stimulated macrophage supernatant at 72 h (Fig. 4G). Moreover, as the core process for tissue healing, type 1 and type 3 collagen fibers were produced from fibroblasts when treated with Da-g-Xan-stimulated macrophage supernatant compared with Da-g-Xan alone (Fig. 4H and Fig. S9C). These experiments demonstrated that the paracrine action of macrophages induced by Da-g-Xan comprehensively amplified the functions of fibroblasts, including migration, proliferation and collagen synthesis (Fig. 4I).

3.5. Da-g-Xan hydrogel adhesive induces M2 macrophages in vivo and protects surgical anastomosis through improving vascularization and collagen deposition

The colonic anastomotic model was developed in rats to test the therapeutic effects of the Da-g-Xan hydrogel adhesive (Fig. 5A). Careful surgical procedures were required to ensure the postoperative survival of the rats, particularly performing the intestinal resection at the ascending colon surrounding the transparent region because this location facilitated to separate blood vessels and reduce bleeding (Fig. S10A). Rats in different groups were left untreated as controls or were treated with by 0.1 mL fibrin gel, or 0.1 mL Da-g-Xan hydrogel adhesive. None of the rats died within 7 d after surgery, and there were no pathological damages to important visceral organs caused by the Da-g-Xan hydrogel adhesive (Fig. S10B).

The measurement of body weight change after surgery presented 4% growth on average in the Da-g-Xan adhesive group, which was more than that in other groups (Fig. S10C), indicating the beneficial role of Da-g-Xan adhesive on the restoration of intestinal food intake without causing intestinal obstruction (Fig. 5B). At POD 7, the abdominal adhesion was evaluated using a site-specific scoring table (Table S3) [42], revealing that the Da-g-Xan hydrogel adhesive was able to reduce the adhesion between anastomosed colon and abdominal wall (Fig. S10D). Moreover, by slow and continuous perfusion of water into colon, the bursting pressure was recorded by using a pressure sensor (Fig. 5C). The results demonstrated that the Da-g-Xan adhesive could strengthen the healing of anastomosed colon, as the rats in this group had the highest bursting pressure (Fig. 5D).

We then wish to know whether the *in vitro* cellular mechanisms proposed in Fig. 4I accounted for the *in vivo* treatment effects. To explore this, we examined the histological changes of anastomotic sites. As shown in Fig. 5E and F, the thickness of regenerated intestinal granulation tissues was higher and the collagen fiber deposition was more obvious in the Da-g-Xan adhesive group than those in other groups. The neovessels were also formed in higher quantities in the Da-g-Xan adhesive group (Fig. 5G). This result implied that the cell functions of fibroblasts and vascular endothelia were enhanced by the Da-g-Xan hydrogel adhesive. Moreover, compared with other groups, the macrophages in the Da-g-Xan adhesive group tended to express more CD206 markers and conduct M2 polarization (Fig. 5H and I), thus reinforcing their paracrine action. Collectively, the above results suggest that Da-g-Xan could induce M2 polarization *in vivo* and create an appropriate microenvironment for tissue repair.

4. Discussion

In this study, we developed a Da-g-Xan hydrogel adhesive based on the functional connections of dopamine and xanthan gum using adhesion components from two marine animals. Owing to the resulting synergistic effects, the contact surface between the adhesive and tissues was enlarged and contained multiple interactions, consequently leading to improvement in the adhesive strength. The unique feature of the adhesive is the dynamic and reversible hydrogen bonds that not only confer diverse advantages such as injectability and self-healing but also allow for a relatively fast erosion rate. The released Da-g-Xan behaves as "a drug" to create a suitable microenvironment for healing of surgical anastomosis by induction of M2 polarization of macrophages through their CD206 surface receptors. Because of this, the fibroblasts and vascular epithelia more actively participated in the colonic anastomosis repair.

Inspiration from natural products has generated artificial products that can be adjusted and enhanced by chemical modification [43]. For example, a simple and feasible conjugation reaction catalyzed by EDC/NHS was used in this study to achieve the conjugate Da-g-Xan. Through increasing the amount of dopamine, the DS was gradually improved and the adhesive strength was correspondingly increased. Moreover, the concentration of Da-g-Xan can also be used to regulate the adhesive strength. These results illustrate the tunable properties of artificial materials. However, chemical modifications add uncertainties to bioinspired materials in regard to keeping the functional and structural characteristics of the natural products. The synthesis process of Da-g-Xan strictly relies on an anaerobic environment filled with nitrogen; otherwise the dopamine will be deteriorated by oxidation [44]. In addition, the conjugation of dopamine may affect the molecular polarity and intermolecular forces of xanthan gum, thus leading to unexpected polymer self-assembly out of the amyloid structure [45]. By careful verification using CD and AFM, we found that the microstructure of Da-g-Xan is more ordered and is analogous to that of the barnacle cement proteins. Therefore, it is important to confirm the functional and structural alterations of polymers whenever there are chemical modifications for the generation of bioinspired materials.

To endow hydrogels with bioactivities, specific drugs are usually encapsulated and sustainably released during *in vivo* application. As for xanthan gum-based hydrogels, previous studies reported the effects of several drugs used to enhance the treatment, including VEGF [46], acyclovir [47], chlorhexidine [48], ibuprofen [49], and omega-3 PUFA [50] for angiogenesis therapy, antiviral therapy, antibacterial therapy, immunoregulatory therapy, and anticancer therapy, respectively. However, it is difficult to synchronize the drug release with hydrogel carrier degradation. Once the degradation is expedited, the bursting drug release will inevitably occur, while if the drug release is too rapid, this increases the risk of hydrogels becoming foreign bodies. Moreover, exogenous growth factor therapies like VEGF, FGF, and TGF-β are not regulated by endogenous negative feedback mechanisms. Therefore, such approaches sometimes lead to tissue hyperplasia and carcinogenic risk [51]. Our study solves these concerns by developing drug-free noncovalent hydrogel therapeutics through direct biorecognition of
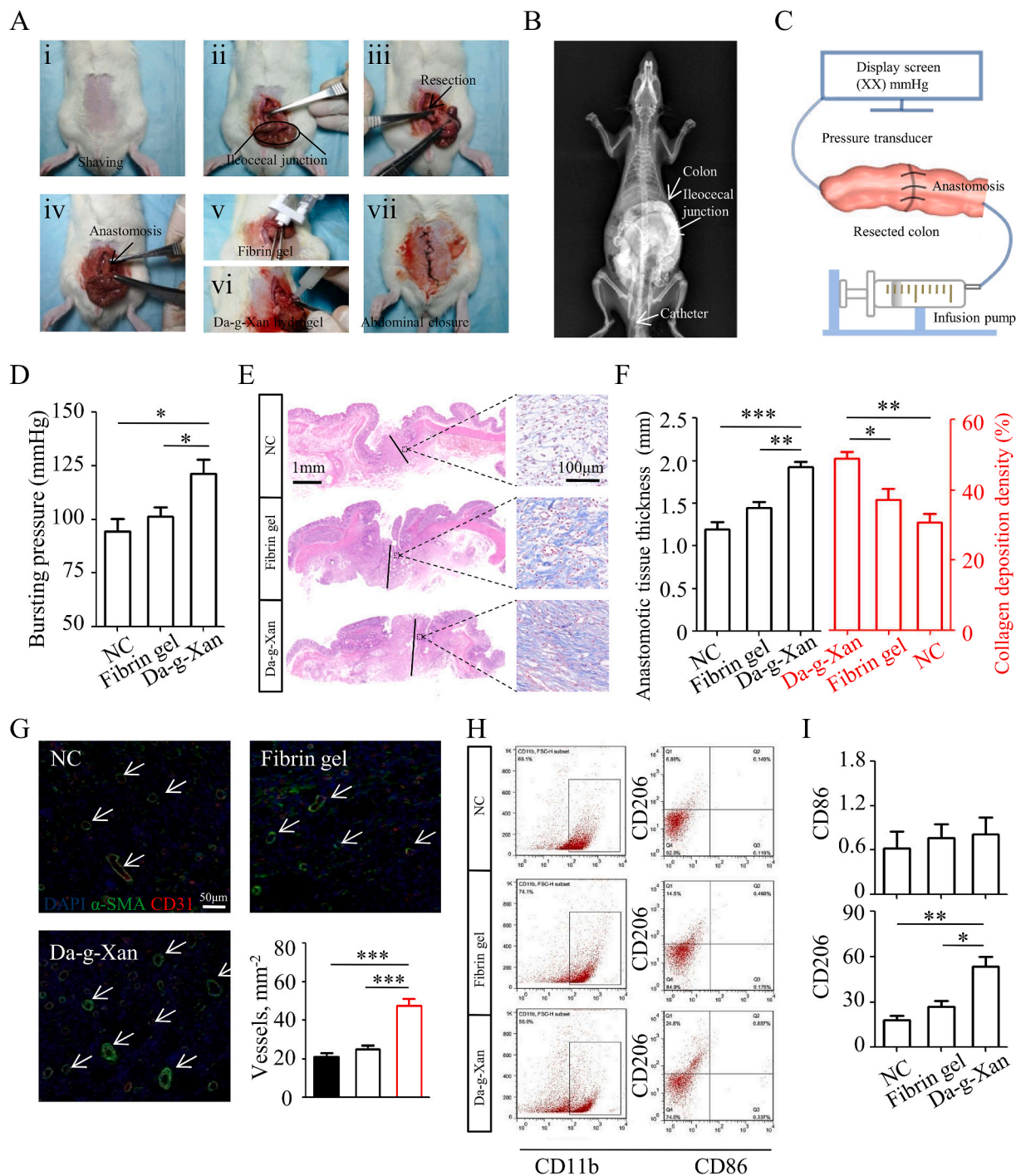
Fig. 5. Da-g-Xan improves the colonic anastomosis healing in a rat model. (A) The specific surgical procedures employed to construct the colonic anastomosis models in rats with different interventions, including simple suture, suture with the fibrin gel protection and suture with the 10%wt Da-g-Xan hydrogel protection. (B) The x-ray imaging indicates that additional treatment by the Da-g-Xan hydrogel adhesive does not cause intestinal obstruction at POD 7. (C) The method used to detect the bursting pressure, which is the highest pressure recorded by a pressure transducer during the continuous infusion of water into the sealed colon. (D) The comparison of bursting pressure by different interventions; n = 5 for each replicate, *p < 0.05. (E) The histological analysis by HE and Masson staining reveals that the healing of colonic anastomosis relies on the regenerated granulation tissues for all interventions, in which the granulation tissues are the thickest with most of the collagen fiber deposition for the Da-g-Xan hydrogel treatment. (F) Quantitative analysis of the granulation tissues and collagen fiber deposition for the different interventions; n = 5 for each replicate, *p < 0.05, **p < 0.01, ***p < 0.001. (G) Quantitative analysis of neovessel formation in regenerated granulation tissues by staining the vascular biomarkers (CD31, α-SMA) for the different interventions; n = 5 for each replicate, ***p < 0.001. (H) The flow cytometry results show that treatment with Da-g-Xan achieves the highest proportion of M2 macrophage polarization in the regenerated granulation tissues among all of the interventions. (I) Quantitative analysis of macrophage polarization proportions for the different interventions, %; n = 5 for each replicate, *p < 0.05, **p < 0.01.

dissolved polysaccharide-derivatives, which highlights the importance of polysaccharides' immunogenicity on designing drug-free hydrogels.

The mannose receptor CD206 has been domenstrated to bind Da-g-Xan and induce M2 polarization of macrophages. Mannose at the side chain of Da-g-Xan may provide the structural basis for recognition by CD206. It was revealed by previous studies that this receptor could

produce anti-inflammatory cytokines either by blocking TLR-4 signaling or by activation using monoclonal antibodies [52,53]. Similarly to the latter approach, our study indicates that Da-g-Xan activates CD206 expression in macrophages and suppresses inflammation, consequently promoting M2 polarization. Moreover, CD206 is an endocytic receptor that mediates the internalization of polysaccharides from the excellular space into the endosomal system for hydrolysis of materials [52]. Consistently, part of Da-g-Xan was found to be intracellularly co-localized with CD206 under the confocal microscope; therefore, it will reduce the risk of foreign body reaction. We believe that CD206 can be a new potential target for the design of mannose-containing biomaterials to accelerate tissue healing.

Beyond the data presented here on the unique material design, physical properties and biological functions of the Da-g-Xan hydrogel adhesive, the bio-safety of xanthan gum authenticated by the U.S. Food and Drug Administration argues favorably for the future clinical translation of this adhesive as a class III medical device. In this way, the product should help patients recover from surgical anastomosis better and faster than before, so that the surgical risks and hospitalization costs will be reduced.

5. Conclusion

Inspired by two marine animals, we developed a Da-g-Xan hydrogel adhesive that simultaneously simulated the mfps and the amyloid-like structure of barnacle cement proteins. This adhesive showed excellent performance in adhering to visceral organ surfaces. The non-covalent interactions with the adhesive enabled rapid erosion and release of Da-g-Xan. This polysaccharide derivative was able to induce M2 polarization of macrophages, creating an appropriate microenvironment for angiogenesis and fibroblast infiltration, thus building the foundation for damage repair of surgical anastomosis. Our current goal is to translate this approach into an injectable and minimally invasive solution for saving numerous patients from suffering the effects of PAL.

CRediT authorship contribution statement

Jinjian Huang: Conceptualization, Funding acquisition, Investigation, Methodology, Software, writing the original draft, Writing - original draft, review & editing & revision, Writing - review & editing. **Yungang Jiang:** Investigation. **Ye Liu:** Investigation. **Yanhan Ren:** Supervision, Validation. **Ziyan Xu:** Investigation. **Zongan Li:** Investigation. **Yun Zhao:** Supervision, Validation. **Xiuwen Wu:** Supervision, Validation, review & editing & revision, Writing - review & editing. **Jianan Ren:** Conceptualization, Funding acquisition, Methodology, Software, Supervision, Validation.

Declaration of competing interest

The authors declared no potential conflicts of interest with respect to the research, authorship, and/or publication of this article.

Acknowledgments

Appendix A. Supplementary data

Supplementary data to this article can be found online at https://doi.org/10.1016/j.bioactmat.2020.09.010.

Data availability

All original data used in this study are available upon request.

References

[1] S.S. Biere, et al., Minimally invasive versus open oesophagectomy for patients with oesophageal cancer: a multicentre, open-label, randomised controlled trial, Lancet 379 (2012) 1887.
[2] F. Wang, et al., Early active drainage by fine tube bundles improves the clinical outcome of anastomotic leak after abdominal surgery: a pilot randomized, controlled trial in two tertiary hospitals in China, Surg. Infect. 20 (2019) 208.
[3] J. Rose, et al., Estimated need for surgery worldwide based on prevalence of diseases: a modelling strategy for the WHO Global Health Estimate, Lancet Glob Health 3 (Suppl 2 S13) (2015).
[4] N.N. Rahbari, et al., Definition and grading of anastomotic leakage following anterior resection of the rectum: a proposal by the International Study Group of Rectal Cancer, Surgery 147 (2010) 339.
[5] R.P. Kiran, A.C. Murray, C. Chiuzan, D. Estrada, K. Forde, Combined preoperative mechanical bowel preparation with oral antibiotics significantly reduces surgical site infection, anastomotic leak, and ileus after colorectal surgery, Ann. Surg. 262 (2015) 416–423.
[6] O. Khan, S. Nizar, G. Vasilikostas, A. Wan, Minimally invasive versus open oesophagectomy for patients with oesophageal cancer: a multicentre, open-label, randomised controlled trial, J. Thorac. Dis. 4 (2012) 465.
[7] X. Li, et al., Nanofiber-hydrogel composite-mediated angiogenesis for soft tissue reconstruction, Sci. Transl. Med. 11 (2019).
[8] J. Huang, Y. Ren, X. Wu, Z. Li, J. Ren, Gut bioengineering promotes gut repair and pharmaceutical research: a review, J. Tissue Eng. 10 (2019) 1013333264.
[9] K.N. Bitar, E. Zakhem, Bioengineering the gut: future prospects of regenerative medicine, Nat. Rev. Gastroenterol. Hepatol. 13 (2016) 543.
[10] K.N. Bitar, S. Raghavan, E. Zakhem, Tissue engineering in the gut: developments in neuromusculature, Gastroenterology 146 (2014) 1614.
[11] P. Sukho, et al., Effects of adipose stem cell sheets on colon anastomotic leakage in an experimental model: proof of principle, Biomaterials 140 (2017) 69.
[12] B.V. Slaughter, S.S. Khurshid, O.Z. Fisher, A. Khademhosseini, N.A. Peppas, Hydrogels in regenerative medicine, Adv. Mater. 21 (2009) 3307.
[13] A.J. Vegas, et al., Combinatorial hydrogel library enables identification of materials that mitigate the foreign body response in primates, Nat. Biotechnol. 34 (2016) 345.
[14] R. Cruz-Acuna, et al., Synthetic hydrogels for human intestinal organoid generation and colonic wound repair, Nat. Cell Biol. 19 (2017) 1326.
[15] J. Wang, F. Zhang, W.P. Tsang, C. Wan, C. Wu, Fabrication of injectable high strength hydrogel based on 4-arm star PEG for cartilage tissue engineering, Biomaterials 120 (2017) 11.
[16] H. Lee, N.F. Scherer, P.B. Messersmith, Single-molecule mechanics of mussel adhesion, Proc. Natl. Acad. Sci. U. S. A. 103 (2006) 12999.
[17] C. Zhong, et al., Strong underwater adhesives made by self-assembling multi-protein nanofibres, Nat. Nanotechnol. 9 (2014) 858.
[18] T.P. Knowles, M.J. Buehler, Nanomechanics of functional and pathological amyloid materials, Nat. Nanotechnol. 6 (2011) 469.
[19] S. Lifson, C. Sander, Antiparallel and parallel β-strands differ in amino acid residue preferences, Nature 282 (1979) 109.
[20] C. Zhang, et al., Engineered Bacillus subtilis biofilms as living glues, Mater. Today 28 (2019) 40.
[21] G.A. Lengyel, W.S. Horne, Design strategies for the sequence-based mimicry of side-chain display in protein β-sheets by α/β-Peptides, J. Am. Chem. Soc. 134 (2012) 15906.
[22] H. Wu, J. Tschopp, S.C. Lin, Smac mimetics and TNFalpha: a dangerous liaison? Cell 131 (2007) 655.
[23] G. Holzwarth, E.B. Prestridge, Multistranded helix in xanthan polysaccharide, Science 197 (1977) 757.
[24] J. Moffat, V.J. Morris, S. Al-Assaf, A.P. Gunning, Visualisation of xanthan conformation by atomic force microscopy, Carbohyd Polym 148 (2016) 380.
[25] M. Krogsgaard, V. Nue, H. Birkedal, Mussel-inspired materials: self-healing through coordination chemistry, Chemistry 22 (2016) 844.
[26] L. Han, et al., Tough, self-healable and tissue-adhesive hydrogel with tunable multifunctionality, NPG Asia Mater. 9 (2017) e372.
[27] P. Martin, S.J. Leibovich, Inflammatory cells during wound repair: the good, the bad and the ugly, Trends Cell Biol. 15 (2005) 599.
[28] L.B. Ivashkiv, Epigenetic regulation of macrophage polarization and function, Trends Immunol. 34 (2013) 216.
[29] A. Kumar, K.M. Rao, S.S. Han, Application of xanthan gum as polysaccharide in tissue engineering: a review, Carbohydr. Polym. 180 (2018) 128.
[30] F. Liu, et al., Immunomodulatory effects of xanthan gum in LPS-stimulated RAW 264.7 macrophages, Carbohyd Polym 169 (2017) 65.
[31] J. Weischenfeldt, B. Porse, Bone marrow-derived macrophages (BMM): isolation and applications, Cold Spring Harb. Protoc. t5080 (2008) 2008.

[32] R. Wang, et al., A biomimetic mussel-inspired ε-Poly-l-lysine hydrogel with robust tissue-anchor and anti-infection capacity, Adv. Funct. Mater. 27 (2017) 1604894.

[33] N.M. Eren, P.H.S. Santos, O. Campanella, Mechanically modified xanthan gum: rheology and polydispersity aspects, Carbohyd Polym 134 (2015) 475.

[34] A. Chauhan, et al., M1 macrophage polarization is dependent on TRPC1-mediated calcium entry, Science 8 (2018) 85.

[35] S. Hadebe, F. Brombacher, G.D. Brown, C-type lectin receptors in asthma, Front. Immunol. 9 (2018) 733.

[36] Z. Hu, Y. Wang, C. Cheng, Y. He, Structural basis of the pH-dependent conformational change of the N-terminal region of human mannose receptor/CD206, J. Struct. Biol. 208 (2019) 107384.

[37] C.T. Gange, et al., Characterization of sugar binding by osteoclast inhibitory lectin, J. Biol. Chem. 279 (2004) 29043.

[38] J. Gan, et al., Producing anti-inflammatory macrophages by nanoparticle-triggered clustering of mannose receptors, Biomaterials 178 (2018) 95.

[39] B. Saha, J.C. Bruneau, K. Kodys, G. Szabo, Alcohol-induced miR-27a regulates differentiation and M2 macrophage polarization of normal human monocytes, J. Immunol. 194 (2015) 3079.

[40] R. Choudhury, et al., The splicing activator DAZAP1 integrates splicing control into MEK/Erk-regulated cell proliferation and migration, Nat. Commun. 5 (2014) 3078.

[41] R.R. Driskell, et al., Distinct fibroblast lineages determine dermal architecture in skin development and repair, Nature 504 (2013) 277.

[42] C. Belluco, et al., Prevention of postsurgical adhesions with an autocrosslinked hyaluronan derivative gel, J. Surg. Res. 100 (2001) 217.

[43] X. Xu, X. Chen, J. Li, Natural protein bioinspired materials for regeneration of hard tissues, J. Mater. Chem. B 8 (2020) 2199.

[44] H.W. Kim, et al., Oxygen concentration control of dopamine-induced high uniformity surface coating chemistry, ACS Appl. Mater. Interfaces 5 (2013) 233.

[45] J.R. Clegg, et al., Modular fabrication of intelligent material-tissue interfaces for bioinspired and biomimetic devices, Prog. Mater. Sci. 106 (2019).

[46] J. Huang, et al., Novel in situ forming hydrogel based on xanthan and chitosan re-gelifying in liquids for local drug delivery, Carbohydr. Polym. 186 (2018) 54.

[47] N.S. Malik, et al., Chitosan/xanthan gum based hydrogels as potential carrier for an antiviral drug: fabrication, characterization, and safety evaluation, Front Chem 8 (2020) 50.

[48] B. Giordani, et al., Freeze-dried matrices based on polyanion polymers for chlorhexidine local release in the buccal and vaginal cavities, J. Pharmacol. Sci. 108 (2019) 2447.

[49] A. Ciric, et al., Study of chitosan/xanthan gum polyelectrolyte complexes formation, solid state and influence on ibuprofen release kinetics, Int. J. Biol. Macromol. 148 (2020) 942.

[50] S. Trombino, S. Serini, R. Cassano, G. Calviello, Xanthan gum-based materials for omega-3 PUFA delivery: preparation, characterization and antineoplastic activity evaluation, Carbohydr. Polym. 208 (2019) 431.

[51] D. Aguilar-Cazares, et al., Contribution of angiogenesis to inflammation and cancer, Front Oncol 9 (2019) 1399.

[52] U. Gazi, L. Martinez-Pomares, Influence of the mannose receptor in host immune responses, Immunobiology 214 (2009) 554.

[53] M. Chieppa, et al., Cross-linking of the mannose receptor on monocyte-derived dendritic cells activates an anti-inflammatory immunosuppressive program, J. Immunol. 171 (2003) 4552.